Applied Surface Science 389 (2016) 790–796

Contents lists available at ScienceDirect

Applied Surface Science

journal homepage: www.elsevier.com/locate/apsusc

Theoretical and experimental study of isothiazolinone adsorption onto ordered mesoporous silica

Lucas E. Mardones[a], María Soledad Legnoverde[a], Sandra Simonetti[b,c], Elena I. Basaldella[a,*]

[a] Centro de Investigación y Desarrollo en Ciencias Aplicadas (CINDECA), Facultad de Ciencias Exactas, Universidad Nacional de La Plata – CONICET Calle 47 N° 257, B1900AJK La Plata, Argentina
[b] Departamento de Física and IFISUR, Universidad Nacional del Sur-CONICET, Av. Alem 1253, 8000 Bahía Blanca, Argentina
[c] Departamentos de Ciencias Básicas e Ingeniería Mecánica, Universidad Tecnológica Nacional, 11 de Abril 461, 8000 Bahía Blanca, Argentina

ARTICLE INFO

Article history:
Received 12 May 2016
Received in revised form 13 July 2016
Accepted 17 July 2016
Available online 19 July 2016

Keywords:
SBA-15
Isothiazolinone
Adsorption

ABSTRACT

Mesoporous silica SBA-15 particles were synthesized in order to evaluate their effectiveness as encapsulating agents for a commercial biocide composed of a mixture of methylisothiazolinone and chloromethylisothiazolinone (MIT/CMIT). Three powdered samples of silica particles having different textural properties, sizes and morphologies were hydrothermally obtained and then characterized by SEM, TEM, SAXS, and nitrogen adsorption–desorption measurements. Adsorption of the biocide on the prepared materials was investigated, and the results showed that adsorption capacities increase as the particle size becomes smaller. Higher biocide amounts were also retained on particles having increased pore size and pore volume. Additionally, a most probable interaction mechanism between MIT/CMIT and SBA-15 is proposed on the basis of molecular modeling calculations. The theoretical approach indicates that two adsorption geometries with comparable minimum levels of strength can be adopted by the biocide: planar adsorption when the biocide molecule rings are adsorbed on the silica surface and vertical adsorption when the O atom of the MIT/CMIT interacts with the H atom of silanols.

1. Introduction

Coatings are usually susceptible to deterioration by a number of different microorganisms (bacteria, fungi or algae), so additives such as biocidal products are essential for the coating formulation. The results of microorganism colonization are the loss of several properties of the product that reduce its performance, generating a negative economic impact and potential health risks.

The presence of microorganisms on the coating surface is related to the degradation of the film (loss of mechanical and aesthetic properties), and also to the risk of transmission of certain diseases.

It is known that the addition of biocides to the coating film contributes to remedying the above-mentioned drawbacks; the substances most commonly used are objected from the point of view of current legislation on environmental matters because most products used in the coating industry are based on isothiazolinones or formaldehyde. Some of these biocides exhibit poor efficiency because of the decrease of their killing power by aging, pH sensitivity, low thermal and alkali stability, etc.

Developments in the field of coatings and modified surfaces include the incorporation of a polymer matrix containing biocides to provide controlled toxicant release. The process consists of a rather complex methodology in which active substances are introduced into a matrix, providing a further release of these active agents, depending on the specific requirements of the substrate on which the matrix is deposited [1–5].

Methylisothiazolinone/chloromethylisothiazolinone (MIT/CMIT) is the active ingredient in a family of commercial microbiocides and preservatives that has a broad spectrum of activity against fungi, yeasts and both gram-positive and gram-negative bacteria [6]. Owing to its high water solubility, MIT/CMIT is prone to leach under humid conditions, resulting in increased concentrations required during initial processing, but this may not be economically or environmentally acceptable. Microencapsulation can contribute to solving these drawbacks by increasing the protection of the active adsorbate from the surrounding environment, or by controlling its release rate into the medium, or by a combination of both.

* Corresponding author.
E-mail addresses: ebasaldella@hotmail.com, eib@quimica.unlp.edu.ar (E.I. Basaldella).

http://dx.doi.org/10.1016/j.apsusc.2016.07.113
0169-4332/

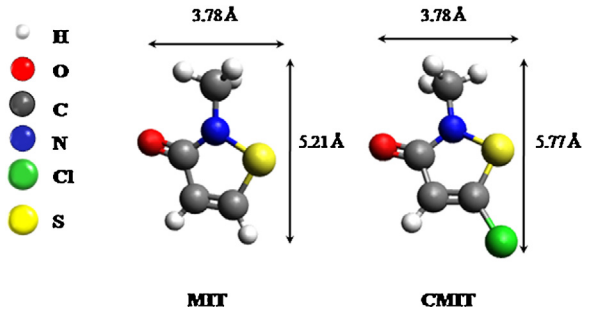

Fig. 1. 3D methylisothiazolinone and chloromethylisothiazolinone molecules.

Several studies are related to bioactive agent encapsulation by using different matrices: polymeric nanoparticles [7–9], microspheres [1,5], porous silica microparticles [10] and modified nanoclay [11]. Regarding the use of mesoporous silica materials for this purpose, the ordered members of the group have recently been proposed as hosts for stabilizing different active agents. Adsorption processes are favored because of an improved ability of these structures to participate as adsorbents, facilitated by their singular surface geometry [12–19]. In particular, in previous work we studied the adsorption of different gases [19–22] and medicinal compounds [23–29] onto these distinctive silica matrices. Additionally, the biocide cations Ag^{+1} and Zn^{+2} were encapsulated in the cavities of an ordered aluminosiliceous framework, and their effective antimicrobial activity after incorporation in different coating formulations was confirmed [30,31].

The main objective of the research presented here is to stabilize organic biocides into micrometer-sized silica particles with a surface that is compatible with coating components and also allow a high biocide loading. Having that in mind, SBA-15 matrices were used for the encapsulation and stabilization of MIT/CMIT, aiming to demonstrate the effective location of the biocide inside the silica pores and to verify that the biocide molecular structure remains unaltered after adsorption. To do this, the biocide location was determined by recording changes in the textural properties of the support during the adsorption process, and the molecular integrity of the adsorbed biocide was determined by FTIR. To go further in this research, the possible interactions of MIT/CMIT with SBA-15 were modeled using a theoretical approach.

2. Materials and methods

2.1. Chemicals

The chemicals used in this study include triblock copolymer poly(ethylene oxide)-poly(propylene oxide)-poly(ethylene oxide) (Pluronic P123, MW: 5800, Aldrich), tetraethyl orthosilicate (TEOS, 98%, Aldrich), hydrochloric acid (HCl, 37%, Anedra).

2.2. Synthesis of materials

SBA-15 materials were synthesized according to the procedure reported by Zhao et al. [32] by using tetraethyl orthosilicate (TEOS; Aldrich) as silica source and Pluronic 123 triblock copolymer (P123, EO20–PO70–EO20; Aldrich) as template. The molar composition used was 1TEOS:4.88HCl:0.0172Pluronic:158.33H_2O. The solution was heated up to 35 °C before adding the TEOS. The resultant solution was stirred at a selected rate (400 rpm) for 20 h at 35 °C, and then the mixture was aged at 80 °C for 24 h under static conditions. The solid product was recovered by filtration and air-dried at room temperature overnight. The template was removed from the as-synthesized material by calcination at 540 °C for 6 h (heating rate = 1 °C min^{-1}). The resultant solid was named SBA_{24}.

The pore size and thickness of the silica wall were adjusted by increasing the time under static conditions of SBA-15 in the reaction solution (48 h). The sample was called SBA_{48}.

Additionally, using the same procedure described for obtaining the sample SBA_{24}, a silica sample having a smaller particle size was obtained by decreasing the stirring rate from 400 to 120 rpm. This sample was named SBA_{120}.

2.3. Materials characterization

The catalysts were characterized by SEM, TEM, SAXS, adsorption–desorption of N_2, and FTIR.

A Philips 505 scanning electron microscope (SEM) was used to perform the morphological analyses of each sample. Transmission electron microscopy (TEM) was performed with a Leo EM-910 instrument operated at 120 kV.

The small angle X-ray scattering (SAXS) measurements were carried out on a model XEUSS 1.0 XENOCS (Grenoble) diffractometer using CuKα radiation (1.5419 A).

Nitrogen adsorption–desorption isotherms were measured at the temperature of liquid nitrogen (−196 °C) using a Micrometrics ASAP 2020 instrument. Before adsorption, samples were outgassed by heating at 100 °C in vacuum, with a pressure lower than 3×10^{-2} mm Hg for 12 h. The surface area was calculated according to the Brunauer–Emmett–Teller (BET) equation. The pore size was obtained by the Barrett-Joyner-Halenda (BJH) method. The pore volume was taken at the $P/P_0 = 0.989$ single point.

Shimadzu IR Affinity-1 equipment, pellets in KBr, and a measuring range of 400–4000 cm^{-1} were used to obtain the FTIR spectra. The samples were placed directly into the chamber, and 48 scans were used for each spectrum.

2.4. Biocide adsorption

In order to evaluate the amount of biocide loaded in the pores of the carrier, 1 g of adsorbent was added to 100 mL of an aqueous solution containing 200 g/L of MIT/CMIT with stirring. After a contact time of 6 h, the solid phases were separated from the liquids by filtration and dried at room temperature. The biocide content in the liquid phases was determined by UV–vis spectroscopy at 274 nm (UV-1800 Shimadzu, Japan).

2.5. Computational method

Calculations were performed with a DFT based code using a Linear Combination of Atomic Orbitals and considering pseudopotentials for the core electrons as implemented in the SIESTA code [33–36] and charge population analysis has been obtained following Bader methodology [37,38]. The interaction between the CMIT/MIT biocide and the silica surface was studied using a two dimensional slab of 168 atoms containing 56 Si, 104 O and 8H atoms, so as to better simulate the semi-infinite nature of the solid surface. A geometry optimization was performed applying relaxation calculations. During the calculations, the structures of both the biocide and the substrate were optimized at convergence in energy of 0.01 eV.

3. Results and discussion

A molecular modeling of methylisothiazolinone and chloromethylisothiazolinone was carried out by employing Avogadro 1.0.0, an advanced molecule editor, arriving at the lower energy configuration shown in Fig. 1.

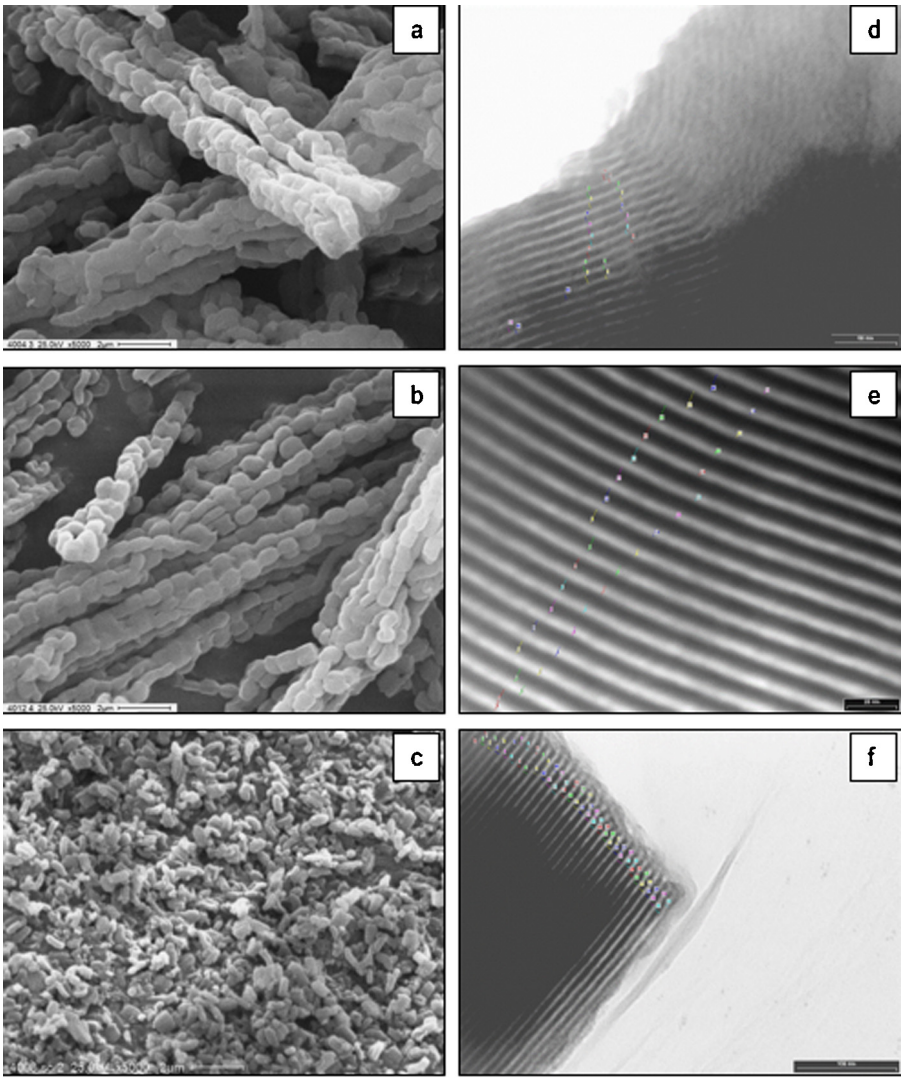

Fig. 2. SEM (a–c) and TEM (d–f) micrographs of SBA_{24} (a and d), SBA_{48} (b and e) and SBA_{120} (c and f).

3.1. Characterization of materials

Scanning electron microscopy (SEM) images (Figs. 2a and b) reveal the typical form of SBA-15 particles as agglomerates with the form of wheat grains composed of small cylinders with relatively uniform sizes of 16–18 μm. By increasing the time under static conditions, the morphology of these solids is well maintained. Nevertheless, a decrease in the stirring rate to 120 rpm significantly decreases the length of particles to ~2 μm (Fig. 2c).

According to Zhao et al. [39], the preparation of materials with a particular morphology is controlled by the rate of agitation of the reaction mixture. Highly energetic organic–inorganic interfaces favor fiber formation, whereas systems with low energy facilitate the formation of curved morphologies for SBA-15 with smaller size. The highly ordered pore structure of synthesized SBA-15 was confirmed by TEM images (Fig. 2 d–f). Mesopore diameters estimated from these TEM images of SBA_{24}, SBA_{48} and SBA_{120} are 49, 61 and 51 nm, respectively. In addition, an average wall thickness can also be measured.

The SAXS patterns for the synthesized mesoporous silicas to show the (100) characteristic reflection associated with the 2D-hexagonal p6 mm structure typical of highly ordered SBA-15 mesoporous structure (Fig. 3). In addition, low-intensity signals can be assigned to directions (110) and (200), indicative of long-range hexagonal ordering. This result is in good agreement with the related TEM results. From Bragg's law for the (100) reflection, one finds that the distance between the centers of adjacent cylin-

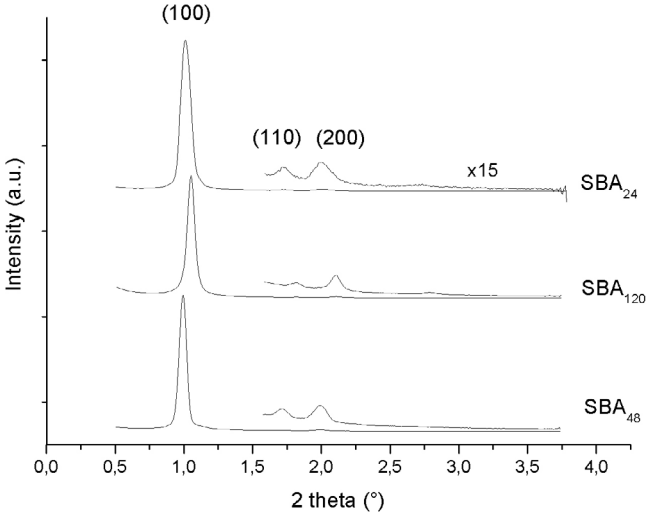

Fig. 3. SAXS patterns of the synthesized SBA-15 samples.

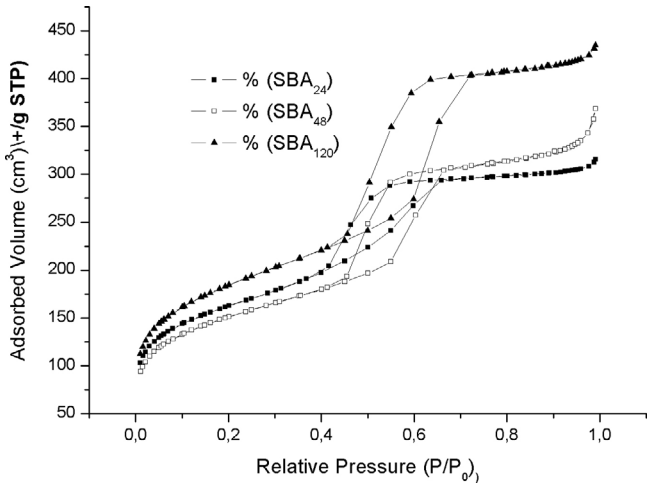

Fig. 4. Nitrogen adsorption and desorption isotherms for silica materials.

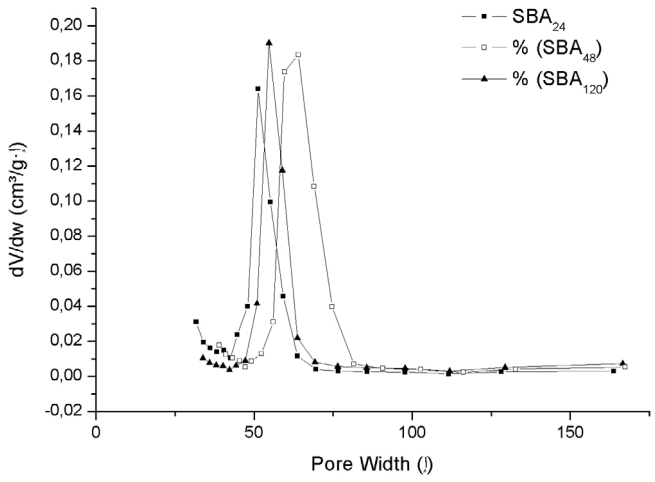

Fig. 5. Pore size distribution (PSD) of silica materials SBA_{24}, SBA_{48} and SBA_{120}.

ders for samples SBA_{24}, SBA_{48}, and SBA_{120} are 87 Å, 89 Å, and 84 Å, respectively. As can be seen in Fig. 4, type IV sorption isotherms according to the IUPAC classification [40] can be observed, with an H1-type hysteresis loop, which is associated with mesoporous materials consisting of well-defined cylindrical-like pore channels. Fig. 5 shows the mesopore size distribution curve calculated by applying the thermodynamic-based BJH method. The desorption branch of the isotherm was used for SBA-15. The textural characteristics of the samples studied are summarized in Table 1.

The aging of as-made SBA-15 in the reaction solution at different times (24 and 48 h) resulted in solids with different pore sizes (51 and 64 Å) and different silica wall thicknesses (49 and 39 Å) (Table 1). As expected, the increase of aging time caused a pore size increase and a decrease of the pore wall thickness [32]. It is also noted that no significant changes in textural properties occurred with the decrease in stirring rates.

Fig. 6 shows the infrared spectra of SBA-15 materials. Asymmetric stretching vibrations of Si—O—Si at 1100 cm^{-1}, symmetric stretching vibrations from Si—O bonds at 800 cm^{-1}, and bending vibrations from Si—O—Si at 456 cm^{-1} are clearly observed. The peaks around 960 cm^{-1} correspond to noncondensed Si OH groups [26,28]. The broad band around 3400 cm^{-1} and the strong peak around 1630 cm^{-1} are due to the stretching and bending vibrations of adsorbed H_2O.

The chemical stability of the biocide after encapsulation was reflected in the IR spectra, where the presence of peaks attributed to isothiazolinones is detected. The bands at 2940, 2890 and 886 cm^{-1} are due to stretching vibrations of C—H, meanwhile bending vibration bands of C—H were observed in the 1450–1390 cm^{-1} range [41].

3.2. Adsorption studies

The influence of the textural properties and particle size of SBA-15 samples on biocide adsorption is shown in Fig. 7. SBA_{120} presents higher adsorption capacity than SBA_{24} and SBA_{48}. It could be inferred that small size particles facilitate the entry of biocide

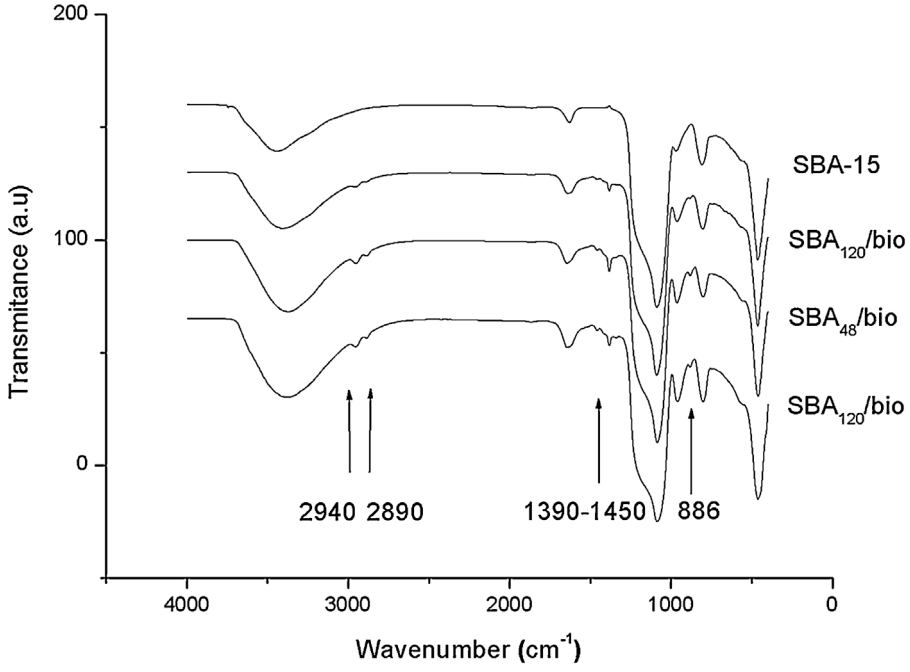

Fig. 6. FTIR spectra of SBA-15 before and after biocide adsorption.

Table 1
Structural properties of SBA-15 samples.

Sample	Reaction time without stirring (h)	Stirring rate (rpm)	d(100) (Å)	S BET (m^2/g)	Pore vol. (cm^3/g)	Pore size (Å)	Wall thickness (Å)
$SBA\text{-}15_{120}$	24	120	84	539	0.51	53	44
$SBA\text{-}15_{24}$	24	400	87	578	0.48	51	49
$SBA\text{-}15_{48}$	48	400	89	658	0.66	64	39

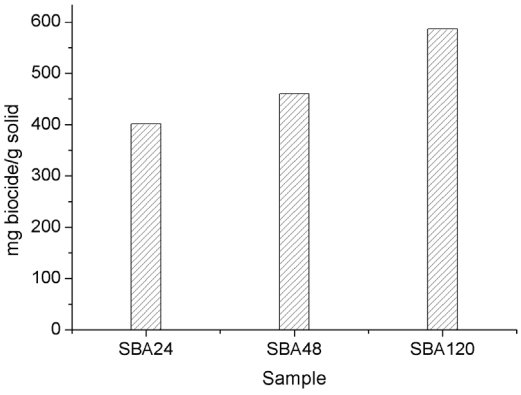

Fig. 7. CMIT/MIT biocide loaded on SBA-15 samples.

Table 2
Adsorption energies according the geometries adopted for CMIT and MIT on silica.

Main molecule-surface interactions	ΔE (eV)
CMIT	
S—OH	−0.04
CH_3—OH	−0.03
N—OH	−0.16
O—OH	−0.36[1]
Cl—OH	−0.04
Ring—OH	−0.42[2]
MIT	
S—OH	−0.05
CH_3 —OH	−0.09
N—OH	−0.08
O—OH	−0.24[3]
Ring—OH	−0.23[4]

[1] G1 geometry in Fig. 8.
[2] G2 geometry in Fig. 8.
[3] G3 geometry in Fig. 9.
[4] G4 geometry in Fig. 9.

into the silica pores, while larger particles lead to slow adsorption abilities of the matrix due not only to the probability of pore blockage by multilayer adsorption at the pore entrance, but also to their increased tortuosity. SBA_{24} and SBA_{48} have similar rod-like morphologies, while the S BET, pore volume and pore size of SBA_{24} are smaller than that of SBA_{48}. It is undoubtedly evident that the particle size is the main factor that markedly affects the adsorption capacity.

3.3. Molecular modeling

To go further in this research, we analyzed the biocide–silica surface interactions using a theoretical approach. The calculations confirmed that CMIT/MIT is adsorbed on the silica surface with comparable levels of strength (see Table 2). The minimum adsorption energies are similar; therefore, several adsorption geometries can be adopted by the biocide; the molecules can adsorb *vertically* on the silica surface (via the different molecule polar groups) or *planar* to the surface (via the molecule ring). Table 2 shows the main molecule–surface interactions according to the different geometries adopted by the molecules during adsorption and the

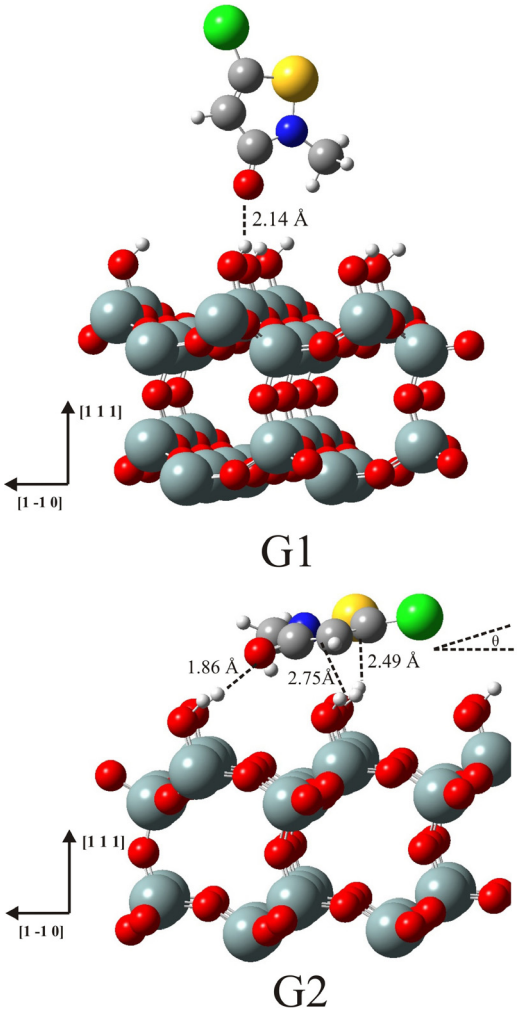

Fig. 8. Most stable CMIT geometries.

corresponding energy of the systems. The most favorable geometries are obtained when the biocide molecule ring adsorbs *planar* on the silica surface (see G2 (Fig. 8) and G4 (Fig. 9)) and, on the other hand, when MIT/CMIT adsorbs *vertically* on silica (the interaction is made between the O atom of the molecules and the H atom of silanols) (see G1 (Fig. 8) and G3 (Fig. 9)). Considering these geometries of minimum energy, the CMIT molecule adsorbs a bit nearer to the surf ace than the MIT molecule; bond distances can be seen in Figs. 8 and 9. On the other hand, the CMIT ring adsorbs on silica forming an angle with the surface plane ($\theta = 11^\circ$); the molecule inclination is not observed during MIT *planar* adsorption ($\theta = 0^\circ$) (compare G2 (Fig. 8) with G4 (Fig. 9)). Considering the same molecule–surface interaction site, the thermodynamics favors CMIT adsorption rather than MIT adsorption, the energy differs between 0.01 and 0.19 eV (see Table 2).

The bonds existing between the biocides and the surface were thought to arise as a result of van der Waals forces and electrostatic interactions. Bader charge analysis shows that the major electron

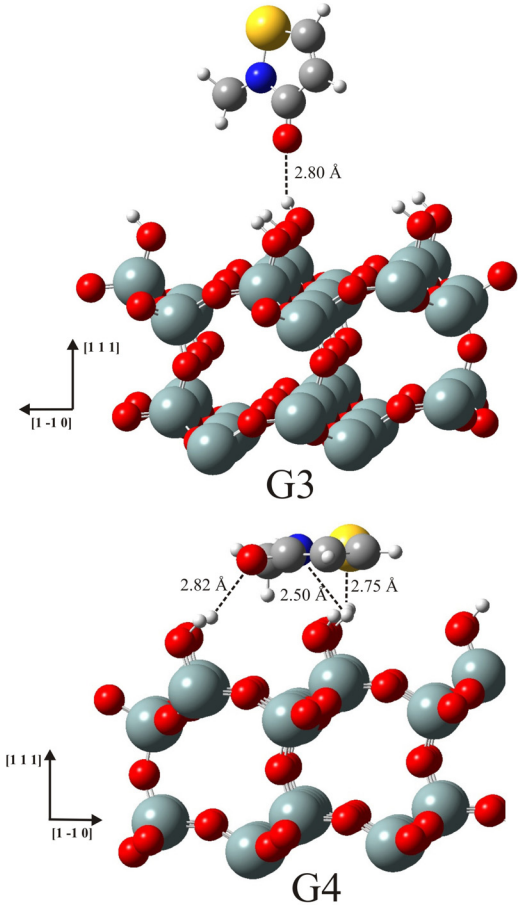

Fig. 9. Most stable MIT geometries.

exchange occurs in O, S and N atoms of the biocide. The electrostatic potentials of O, S and N atoms are essentially negative. However, the silica matrix has an essentially positive electrostatic potential. For this reason, CMIT and MIT molecules can interact with the surface through H atoms of the silanol groups of silica. When the biocide molecules are adsorbed, hydrogen bonds are made with surface silanols; while the ring and methyl group of the biocide contribute to stabilizing the negative charge of Si—O—Si groups of the silica surface. This could be due to the orientation of the biocide molecules as they adsorb onto the silica, with the more positive groups of biocide interacting via dispersive interactions, whereas the negative charged atoms of CIT/MIT participate in the adsorption process via H-bond interactions.

4. Conclusions

Encapsulation of a commercial isothiazolinone-based biocide in mesoporous silica materials with different pore sizes and morphologies has been attained, preserving the original molecular integrity of the adsorbed molecules. The influence of differences in textural properties as well as morphology and particle size of the carrier materials on the adsorption capacity was evaluated. Adsorption results mainly depended on the particle size of the silica support. SBA-15 particles of the smallest size encapsulated the largest amount of biocide, due to decreased tortuosity. By reducing the particle size, adsorption capacities as high as 600 mg biocide/g silica were obtained. Besides, two probable interaction mechanisms between MIT/CMIT and SBA-15 were determined on the basis of molecular modeling calculations. The most favorable geometries adopted by the biocide in the adsorption on SBA-15 were planar, if the interactions were made between the biocide molecule ring and the silica surface, and vertical, if the interactions were made between the O atom of MIT/CMIT and the H atom of silanols.

Acknowledgments

The authors would like to thank CIC, ANPCyT and CONICET for financial support.

References

[1] L. Nordstierna, A.A. Abdalla, M. Masuda, G. Skarnemark, M. Nydén, Molecular release from painted surfaces: free and encapsulated biocides, Prog. Org. Coat. 69 (2010) 45–48.
[2] F. Maia, A.P. Silva, S. Fernandes, A. Cunha, A. Almeida, J. Tedim, M.L. Zheludkevich, M.G.S. Ferreira, Incorporation of biocides in nanocapsules for protective coatings used in maritime applications, Chem. Eng. J. 270 (2015) 150–157.
[3] V. Bekiari, K. Nikolaou, N. Koromilas, G. Lainioti, P. Avramidis, G. Hotos, J.K. Kallitsis, G. Bokias, Release of polymeric biocides from synthetic matrices for marine biofouling applications, Agric. Agric. Sci. Procedia 4 (2015) 445–450.
[4] Z. Sun, L. Gu, J. Zheng, J. Zhang, L. Wang, F. Xu, C. Lin, A controlled release strategy of antifouling agent in coating based on intercalated layered double hydroxides, Mater. Lett. 172 (2016) 105–108.
[5] M. Andersson Trojer, L. Nordstierna, J. Bergek, H. Blanck, K. Holmberg, M. Nydén, Use of microcapsules as controlled release devices for coatings, Adv. Colloid Interface Sci. 222 (2015) 18–43.
[6] J. Fewingasn, T. Menne, An update of the risk assessment for methylchloroisothiazolinone/methylisothiamlinone (MCUMI) with focus on rinse-off products, Contact Dermat. 41 (1999) 1–13.
[7] Y. Liu, P. Laks, P. Heiden, Controlled release of biocides in solid wood. II. Efficacy against Trametes versicolor and Gloeophyllum trabeum wood decay fungi, J. Appl. Polym. Sci. 86 (2002) 608–614.
[8] Y. Liu, L.P. Yan, P. Heiden, P. Laks, Use of nanoparticles for controlled release of biocides in solid wood, J. Appl. Polym. Sci. 79 (2001) 458–465.
[9] Y. Liu, P. Laks, P. Heiden, Controlled release of biocides in solid wood. III. Preparation and characterization of surfactant-free nanoparticles, J. Appl. Polym. Sci. 86 (2002) 615–621.
[10] G. Sørensena, A.L. Nielsena, Morten Møller Pedersena, S. Poulsenb, H. Nissenc, M. Poulsena, S.D. Nygaard, Controlled release of biocide from silica microparticles in wood paint, Prog. Org. Coat. 68 (2010) 299–306.
[11] J. Eversdijk, S.J.F. Erich, S.P.M. Hermanns, O.C.G. Adan, M. De Bolle, K. de Meyer, D. Bylemans, M. Bekker, A.T. ten Cate, Development and evaluation of a biocide release system for prolonged antifungal activity in finishing materials, Prog. Org. Coat. 74 (2012) 640–644.
[12] Q.Z. Zhai, W.H. Hu, B.L. Huang, C.Y. Wang, Synthesis and characterization of mesoporous SBA-15/propranolol hydrochloride for controlled drug release study, J. Sol-Gel Sci. Technol. 63 (2012) 435–444.
[13] M. Moritz, M.a Geszke-Moritz, Application of nanoporous silicas as adsorbents for chlorinated aromatic compounds. A comparative study, Mater. Sci. Eng. C 41 (2014) 42–51.
[14] C. Perego, R. Millini, Porous materials in catalysis: challenges for mesoporous materials, Chem. Soc. Rev. 42 (2013) 3956–3976.
[15] M. Moritz, M. Łaniecki, SBA-15 mesoporous material modified with APTES as the carrier for 2-(3-benzoylphenyl)propionic acid, Appl. Surf. Sci. 258 (2012) 7523–7529.
[16] V. Hernández-Morales, R. Nava, Y.J. Acosta-Silva, S.A. Macías-Sánchez a, J.J. Pérez-Bueno, B. Pawelec, Adsorption of lead (II) on SBA-15 mesoporous molecular sieve functionalized with NH2 groups, Micropor. Mesopor. Mater. 160 (2012) 133–142.
[17] S. Park, P. Pendleton, Mesoporous silica SBA-15 for natural antimicrobial delivery, Powder Technol. 223 (2012) 77–82.
[18] I. Izquierdo-Barba, S. Sánchez-Salcedo, M. Colilla, M.J. Feito, C. Ramírez-Santillán, M.T. Portolés, M. Vallet-Regí, Inhibition of bacterial adhesion on biocompatible zwitterionic SBA-15 mesoporous materials, Acta Biomater. 7 (2011) 2977–2985.
[19] T. Xuan Bui, H. Choi, Adsorptive removal of selected pharmaceuticals by mesoporous silica SBA-15, J. Hazard. Mater. 168 (2009) 602–608.
[20] C.A. Grande, N. Firpo, E.I. Basaldella, A.E. Rodrigues, Propane/propene separation by SBA-15 and Ð-complexated Ag-SBA-15, Adsorption 11 (2005) 775–780.
[21] E.I. Basaldella, J.C. Tara, G. Aguilar Armenta, M.E. Patiño-Iglesias, Cu/SBA-15 as adsorbent for propane/propylene separation, J. Porous Mater. 14 (2007) 273–278.
[22] E.I. Basaldella, M.S. Legnoverde, E.N. Ponzi, J.C. Tara, N. Firpo, E.L. Soto, Amine modified, micro-mesoporous matrices for CO2 retention: effect of occluded templates on performance, Stud. Surf. Sci. Catal. 174A (2008) 619–622.
[23] T. López, E.I. Basaldella, M.L. Ojeda, R. Alexander-Katz, Encapsulation of valproic acid and sodic phenytoine in ordered mesoporous SiO2 solids for the treatment of temporal lobe epilepsy, Opt. Mater. 29 (2006) 75–81.
[24] T. López, E. Krötzsch, E. Ortiz-Islas, M. Alvarez-Lemus, E. Basaldella, J.M. Martínez-Blanes, J.A. Odriozola, Release properties and acute biosecurity

determination of collagen-polyvinylpyrrolidone loaded in ordered mesoporous silica, Key Eng. Mater. 391 (2009) 169–184.
[25] T. Lopez, E. Ortiz, R. Alexander-Katz, E.I. Basaldella, X. Bokhimi, Cortisol controlled release by mesoporous silica, Nanomed.: Nanotechnol. Biol. Med. 5 (2009) 170–177.
[26] E.I. Basaldella, M.S. Legnoverde, Functionalized silica matrices for controlled delivery of cephalexin, J. Sol-Gel Sci. Technol. 56 (2010) 191–196.
[27] T. López, E. Ortiz, D. Meza, E. Basaldella, X. Bokhimi, C. Magaña, A. Sepúlveda, F. Rodríguez, J. Ruiz, Controlled release of phenytoin for epilepsy treatment from titania and silica based materials, Mater. Chem. Phys. 126 (2011) 922–929.
[28] M.S. Legnoverde, I. Jiménez-Morales, E. Rodríguez-Castellón, A. Jiménez-Morales, E.I. Basaldella, Modified silica matrices for controlled release of cephalexin, Med. Chem. 9 (2013) 672–680.
[29] M.S. Legnoverde, S. Simonetti, E.I. Basaldella, Influence of pH on cephalexin adsorption onto SBA-15 mesoporous silica. Theoretical and experimental study, Appl. Surf. Sci. 300 (2014) 37–42.
[30] A.M. Pereyra, M.R. Gonzalez, V.G. Rosato, E.I. Basaldella, A-type zeolite containing Ag+/Zn2+ as inorganic antifungal for waterborne coating formulations, Prog. Org. Coat. 77 (2014) 213–218.
[31] A.M. Pereyra, M.R. Gonzalez, T.A. Rodrigues, M.T. Soares Luterbach, E.I. Basaldella, Enhancement of biocorrosion resistance of epoxy coating by addition of Ag/Zn exchanged A zeolite, Surf. Coat. Technol. 270 (2015) 284–289.
[32] D. Zhao, Q. Huo, J. Feng, B.F. Chmelka, G.D. Stucky, Triblock copolymer syntheses of mesoporous silica with periodic 50 to 300 Angstrom pores, Science 279 (1998) 548–552.
[33] J.M. Soler, E. Artacho, J.D. Gale, A. Garcia, J. Junquera, P. Ordejon, D. Sanchez-Portal, The SIESTA method for ab initio order materials simulation, J. Phys. Condens. Matter 14 (2002) 2745–2779.
[34] D. Sánchez-Portal, P. Ordejon, E. Canadell, Computing the properties of materials from first principles with SIESTA, Struct. Bond. 113 (2004) 103–170.
[35] N. Troullier, J.L. Martins, Efficient pseudopotentials for planewave calculations, Phys. Rev. B 43 (1991) 1993–2006.
[36] H.J. Monkhorst, J.D. Pack, Special points for Brillouin-zone integrations, Phys. Rev. B 13 (1976) 5188–5192.
[37] R. Bader, Atoms in Molecules: A Quantum Theory, University Press, New York: Oxford, 1990.
[38] G. Henkelman, A. Arnaldsson, H. Jónsson, A fast and robust algorithm for Bader decomposition of charge density, Comput. Mater. Sci. 36 (2006) 354–360.
[39] D. Zhao, J. Sun, Q. Li, G.D. Stucky, Morphological control of highly ordered mesoporous silica SBA-15, Chem. Mater. 12 (2000) 275–279.
[40] K.S.W. Sing, D.H. Everett, R.A.W. Haul, L. Moscou, R.A. Pierotti, J. Rouquerol, T. Siemieniewska, Reporting physisorption data for gas/solid systems with special reference to the determination of surface area and porosity, Pure Appl. Chem. 57 (1985) 603–619.
[41] G. Mille, J.L. Meyer, J. Chouteau, Δ-2 thiazoline et alkyl-2 Δ-2 thiazolines: etude vibrationnelle infrarouge et raman conformation, J. Mol. Struct. 50 (1978) 247–257.